Journal of Glaciology

Article

Cite this article: Colucci RR *et al*. (2026) ^{39}Ar dating of cave ice combined with pollen, cryogenic calcite and radiocarbon analyses reveals late Little Ice Age origin (Leupa Ice Cave, Julian Alps). *Journal of Glaciology* **72**, e18, 1–15. https://doi.org/10.1017/jog.2026.10125

Received: 29 July 2025
Revised: 9 December 2025
Accepted: 1 January 2026

Keywords:
cave ice; ice chronology/dating; ice core

Corresponding author:
Renato R. Colucci;
Email: renato.colucci@cnr.it

*now at Alfred-Wegener-Institute Helmholtz Zentrum für Polar- und Meeresforschung, Bremerhaven - Germany
**now at Civil Protection of the Autonomous Region of Friuli Venezia Giulia - Italy.

^{39}Ar dating of cave ice combined with pollen, cryogenic calcite and radiocarbon analyses reveals late Little Ice Age origin (Leupa Ice Cave, Julian Alps)

Renato R. Colucci[1,2], Pascal Bohleber[3,4,*], Werner Aeschbach[5], Marc Luetscher[6], Margit Schwikowski[7,8,9], Gina E. Moseley[10], David Wachs[5,11], Theo Manuel Jenk[7,8], Anja Eichler[7,8], Andrea Securo[1,4], Lawrence R. Edwards[12], Sonia Manzan[13,**], Dirk L. Hoffmann[14], Markus K. Oberthaler[11] and Daniela Festi[15]

[1]Institute of Polar Sciences, National Research Council, Trieste, Italy; [2]Alpine-Adriatic Meteorological Society, Udine, Italy; [3]Institute for Interdisciplinary Mountain Research, Austrian Academy of Sciences, Innsbruck, Austria; [4]Department of Environmental Sciences, Informatics and Statistics, Ca'Foscari University of Venice, Venice, Italy; [5]Institute of Environmental Physics, Heidelberg University, Heidleberg, Germany; [6]Swiss Institute for Speleology and Karst Studies (SISKA), La Chaux-de-Fonds, Switzerland; [7]PSI Center for Energy and Environmental Sciences, Villigen PSI, Willigen, Switzerland; [8]Oeschger Centre for Climate Change Research, University of Bern, Bern, Switzerland; [9]Department of Chemistry, Biochemistry and Pharmaceutical Sciences, University of Bern, Bern, Switzerland; [10]Institute of Geology, University of Innsbruck, Innsbruck, Austria; [11]Kirchhoff-Institute for Physics, Heidelberg University, Heidelberg, Germany; [12]University of Minnesota, Earth Sciences, Minneapolis, MN, USA; [13]Department of Mathematics and Geosciences, University of Trieste, Trieste, Italy; [14]Geoscience Center, Geochemistry and Isotope Geology Department, University of Göttingen, Göttingen, Germany and [15]GeoSphere Austria, Department of Geoanalytics and Reference Collections, Vienna, Austria

Abstract

High-latitude or high-altitude caves often preserve ice deposits that contain valuable signals of past climate conditions, sometimes even reflecting regional and local atmospheric variability. Phases of aggradation or degradation of underground ice can also provide insights into the temporal evolution of Alpine permafrost. Such data are typically obtained from ice cores, which require a well-constrained chronological framework to be meaningful. In recent years, several dating methods have been developed or refined for glacier and ice sheet cores. However, some of these techniques have not yet been applied to cave ice. In this study, the ^{39}Ar dating technique using Argon Trap Trace Analysis is applied for the first time to an underground ice deposit in the south-eastern Alps, specifically in the Canin-Kanin massif (Julian Alps). The results are compared with pollen markers extracted from the ice, with U-Th dating of cryogenic cave carbonates found in situ within the same ice block, and with radiocarbon (^{14}C) dating of the water-insoluble organic carbon fraction embedded in the ice. This integrated approach enabled dating the ice deposit to the end of the Little Ice Age, at the onset of the subsequent warming phase.

1. Introduction

Ice caves and lava tubes hosting perennial ice accumulations are widely considered as evidence for sporadic permafrost (Holmlund and others, 2005). Such a view has recently been supported by long-term observations of the thermal state of the rock at different depths, previously poorly known (e.g., Luetscher and Jeannin, 2004; Perşoiu and Pazdur, 2011; Colucci and Guglielmin, 2019). With permafrost we refer to, by definition, any material with a temperature less or equal to 0°C for at least two consecutive years. Ice in caves is described as a global phenomenon and found in most, if not all, climatic zones: from polar and subarctic regions (e.g., Lauritzen, 2006; Yonge and others, 2018) to the Mediterranean (e.g., Kern and others, 2011; Oliva and others, 2018) and even in hot arid climate areas (e.g., Karimi Vardanjani and others, 2017; Kadebskaya and Mavlyudov, 2018). In the Alps, the presence of ice in caves has been well documented and known for centuries. It is reported by Brevini and others (2004) how Leonardo Da Vinci took some notes in his personal diary by the end of the 1400s, describing the characteristics of ice deposits of a cave in the Alps, likely in the Grigna sector (Maggi and others, 2018), southern Alps.

The distribution and volumes of alpine underground ice remain poorly quantified. However, recent studies have suggested the existence of thousands of caves hosting ice across the entire

https://doi.org/10.1017/jog.2026.10125 Published online by Cambridge University Press

mountain range (Persoiu and Lauritzen, 2017; Maggi and others, 2018). The general processes leading to the formation and preservation of permanent cave ice deposits are well known (Luetscher and Jeannin, 2004), and recent numerical models describing heat exchange between ice, cave air and rock have been proposed (Bertozzi and others, 2019). Yet, each cave presents unique characteristics owing to the complexity of each karst system. In general, ice in caves can accumulate by freezing of liquid water, snow drift and, to a lesser extent, by condensation of moist air at sub-zero temperatures (Luetscher and Jeannin, 2004; Perşiu and others, 2017). Recent studies conducted in the Southeastern Alps gave a rather comprehensive overview of both cave cryosphere peculiarities in this specific alpine sector (Colucci, 2016; Colucci and Guglielmin, 2019), residual glaciers and ice patches (Colucci, 2016; Colucci and Žebre, 2016; Colucci and others, 2021) and recent climatic evolution (Colucci and others, 2017a). Lately, cave ice has provided valuable Holocene climate proxy records as well (Kern and others, 2011; Spötl and Cheng, 2014; Perşiu and others, 2017; Sancho and others, 2018), highlighting the importance of reliable age information to reconstruct periods of net ice mass gain, ice stagnation or ice loss in order to interpret such information from a palaeoclimatic perspective. In this context, the impact of Holocene climate phenomena such as the Little Ice Age (LIA) is of particular interest.

Recently, Racine and others (2022) produced a chronological synthesis in the Eastern Alps based on 107 radiocarbon dates collected from eight sag-type ice caves, that is, systems in which snow accumulation from precipitation is the main parameter controlling the mass balance. When these data were compared with the known history of past Alpine glacier advances, they showed an excellent correlation. This is consistent with findings from the Canin area by Securo and others (2022a), who related the recent decades of evolution of the local underground cryosphere to the behaviour of nearby ice patches.

In contrast to ice core drilling sites of sedimentary ice bodies like glaciers, offering to some extent the option of annual layer counting, cave ice age information typically comes from radiometric dating, pollen time markers, dendrochronology of stems and cryoclasts, including archaeological artefacts. However, there are exceptions where the annual layering of cave ice can be used (Borsato and others, 2004). First attempts of dating underground ice deposits were made with pollen (Kral, 1968; Schmeidl and Kral, 1969) in the eastern Alps. This method provides more information if, for example, a given pollen assemblage may provide an absolute age range. This might be the case of, for example, pollen of neophytes and crops for which the introduction date to Europe is known. Regarding radiometric ice dating, important advances have been made in applying and refining the application of the radiocarbon dating method to the particulate organic carbon fraction preserved in ice (Uglietti and others, 2016; Hoffmann and others, 2018b; Fang and others, 2021). Only recently, the use of sophisticated Atom Trap Trace Analysis (ATTA) has provided the break-through in using ^{39}Ar for glacier ice dating (Feng and others, 2019; Ritterbusch and others, 2022; Hou and others, 2025).^{39}Ar is a unique tracer for dating environmental water and ice bodies within the age range of 100–1000 years, thus making it an invaluable addition to the radiometric ice dating toolbox. In cave ice deposits, a special opportunity arises from layers of cryogenic cave carbonates (CCCs) (Žák and others, 2004, 2008; Luetscher and others, 2013; Spötl and Cheng, 2014; Munroe and others, 2021; Töchterle and others, 2022). These low-Mg calcite minerals appear as tiny crystals in layered ice and resemble dust layers (Lauriol and Clark, 1993). Their distinct stable isotope signatures suggest they form through CO_2 degassing and rapid freezing of thin water films on ice. Unlike larger pool-formed coarse CCC, fine CCC crystallize simultaneously with the ice, so their radiometric dating generally determines the age of the ice. A first attempt using radiocarbon was made in two Canadian Arctic caves (Lauriol and Clark, 1993), but follow-up studies are lacking. Uranium–thorium dating, though effective for coarse CCC, is more difficult for fine CCC due to low ^{230}Th/^{232}Th ratios and detrital contamination (Luetscher and others, 2013; Spötl and Koltai, 2025). Only one successful application to fine CCC has been reported, from a cave in NE Greenland (Donner and others, 2023).

Another method involves using radiocarbon (^{14}C) to date the water-insoluble organic carbon (WIOC) fraction embedded in the ice. This methodology has recently become an established tool for constraining the age scale of ice core archives from high-altitude glaciers (Jenk and others, 2007; Sigl and others, 2009; Uglietti and others, 2016; Hoffmann and others, 2018b) and is now widely applied (e.g., Jenk and others, 2009; Gabrielli and others, 2016; Hou and others, 2018; Fang and others, 2023). Limitations of this approach become relevant if the WIOC concentrations in the ice are particularly low, typically below a threshold of available carbon amounts $< 10\mu$g C (Uglietti and others, 2016; Dyonisius and Jenk, 2025). In such contexts, an efficient alternative is dating of the dissolved organic carbon (DOC), which has typically higher concentrations than the WIOC fraction (Fang and others, 2021). However, due to its solubility, this fraction is not suitable for dating of temperate ice bodies, where the DOC, at least partly, will be removed by percolating melt water. Here the WIOC fraction was therefore used for dating.

The decline of cave ice deposits is a widespread phenomenon that calls for urgent scientific actions aimed at saving and archiving as much information as possible before the ice completely melts away (Kern and Perşoiu, 2013).

The aims of this work are: (i) to date part of an existing underground ice body in the Leupa Ice Cave and investigate possible links with the regional glaciation history; (ii) to apply the ^{39}Ar dating method to cave ice, a technique that has never been used in this context before; and (iii) to compare the obtained results with other dating methods previously applied in caves, such as the presence of pollen markers, and U-Th on CCC.

2. Study site

Leupa Ice Cave is located in the Julian Alps (southeastern European Alps; 46°21′N, 13°26′E, Fig. 1) and opens at 2285 m a.s.l. on the North Side of Mount Leupa (2402 m). In the area, the presence of a few very small snow and ice patches, mainly located at the foot of northern rock walls, results from the very high mean annual precipitation (3335 mm) and avalanche activity (Colucci and Žebre, 2016; Colucci and others, 2016b). A glaciokarst landscape sensu Žebre and Stepišnik (2016) is predominant, and the prevalent lithologies are dolostones and limestones of the Norian-Rhaetian platform. The area is characterized by a large number of caves hosting ice deposits with median elevations of the entrances at 1871 m a.s.l. (Colucci and others, 2016b). The 2011–19 Leupa Ice Cave air temperature shows a mean value of –0.91°C (extremes –12.1°C and 2.9°C). The mean annual air temperature (MAAT) at 2200 m a.s.l. (1981-2010 period) in the Canin-Kanin massif is 1.1°C (Colucci and Guglielmin, 2015). The altitude of the mean annual 0°C isotherm is estimated at 2370 $\pm$ 90 m, which means roughly 100 m higher than the main Leupa Ice Cave entrance (Colucci and others, 2016a).

https://doi.org/10.1017/jog.2026.10125 Published online by Cambridge University Press

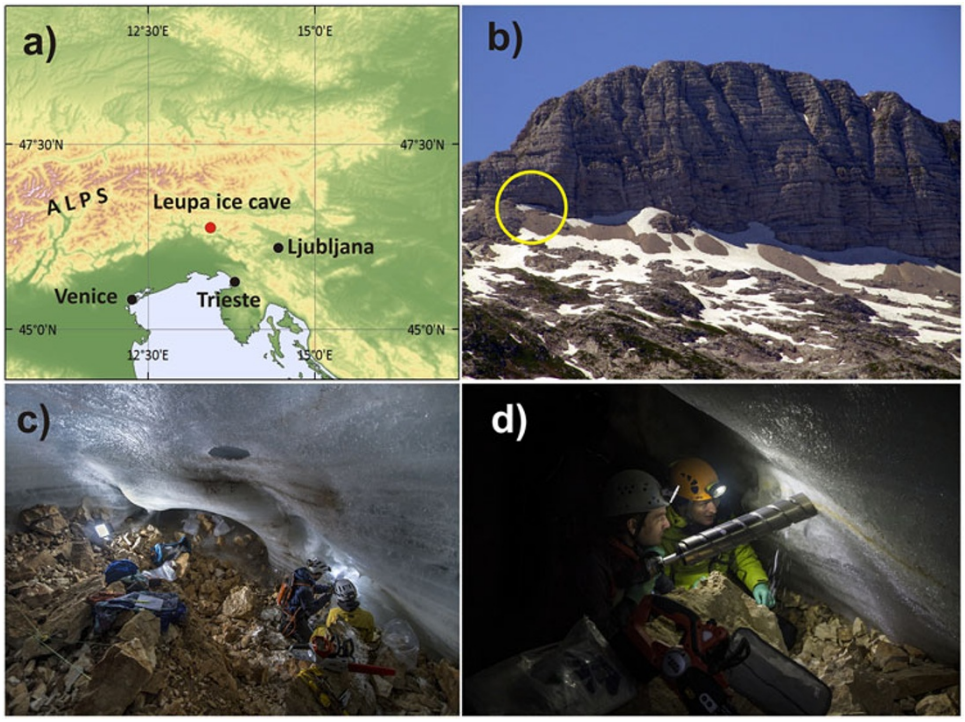

Figure 1. Overview of the study area and the Leupa Ice Cave. (a) Location of Leupa Ice Cave in the eastern European Alps. This map was designed with the software ArcMap version 10.1 and is based on digital elevation information from the Shuttle Radar Topography Mission (http://srtm.csi.cgiar.org), further edited using the CorelDRAW graphic suite, release X3 (http://www.corel.com). (b) The entrance of the Leupa Ice Cave located on the north face of Mount Leupa. (c,d) The ice outcrop within the ice chamber during the phase of sampling on 9 November 2016 and 3 October 2018.

The Leupa Ice Cave (Julian Alps) has been known since the 1970s (Mikolic, 1979) and is one of the most intensively studied alpine ice caves during the last 15 years (Colucci and others, 2016b; Bertozzi and others, 2019; Colucci and Guglielmin, 2019; Securo and others, 2022b). Moreover, a layer of CCC was found in situ in the permanent ice deposit (Colucci and others, 2017b) in 2016. Leupa Ice Cave offers the opportunity to directly compare a range of state-of-the-art ice dating methods specifically for their merit for dating cave ice, with the special target to constrain the age of the ice (or at least part of it) at this site. Recently, a 2D temperature evolution in the rock walls of the Leupa Ice Cave has been reconstructed, and shows the development of a 29–44 m thick layer of permafrost in the north face of Mount Leupa during the LIA, eventually favouring the freezing of percolation water in the voids (Colucci and Guglielmin, 2019). With post-LIA warming, the impact of cave air circulation became significant in preserving sporadic permafrost in the rock hosting the cave ice deposit until the almost complete permafrost degradation occurred in 2014. At the present condition (2024), an almost complete degradation of permafrost occurred, and the ice deposit is undergoing an abrupt and dramatic retreat (Securo and others, 2022b).

The Leupa Ice Cave is located above the timberline in a terrain characterized by very steep rocky slopes that allow the development of vegetation mainly in the cracks. Only a few plant species have been observed to grow sporadically around the cave entrance, mainly *Arabis alpina* L. (alpine rock-cress), *Saxifraga oppositifolia* L. (purple saxifrage), *Saxifraga sedoides* L., *Poa alpina* L. (alpine bluegrass) and the fern *Cystopteris alpina* (Lam.) Desv. Mosses also develop locally, forming small cushions. The timberline located at 1750 m elevation is formed by *Pinus mugo Turra (*mountain pine), while the subalpine belt is characterized by larch and spruce forest, where larch (*Larix decidua* Mill.) dominates over spruce (*Picea abies* (L.) H. Karst.). Due to the scarcity of vegetation near the cave, we anticipate that the pollen spectra record will be representative of the regional vegetation composition. At the time of the ice coring, the cave hosted a roughly 300 m^3 sub-horizontal and layered ice body averaging ~3 m in thickness.

The existence of at least three entrances at different altitudes leads to a complex airflow system with a seasonally reversed direction (Bertozzi and others, 2019), where forced convection induced by internal–external temperature contrasts is the most significant mechanism (Wigley and Brown, 1976; Luetscher and Jeannin, 2004). The 8 year (2012–20) ice body volume change has been recently quantified through a photogrammetric approach combined with ground penetrating radar surveys (Securo and others, 2022b), resulting in a loss of more than 180 m^3. The combined action of surface melting from above and below the main ice deposit led to the formation of a superficial hole during the ablation season of 2021 (Fig. 2). This event drastically changed the air circulation in the cave.

3. Methods

The ice sampling for dating (Fig. 2) was carried out in two different field campaigns (2016 and 2018). The sampling for ^{39}Ar dating was performed on 3 October 2018, with a battery-powered chain saw in order to obtain several large ice blocks of at least 4 kg each. Three different sampling locations were selected, including the CCC layer as well as positions above and below it (^{39}Ar-1, ^{39}Ar-2 and ^{39}Ar-3). Ice sampling for pollen analysis was carried out on 3 October 2018. Three decimetric ice blocks along a vertical transect (i) from the surface of the ice body (P-1), (ii) from the layer including cryogenic

https://doi.org/10.1017/jog.2026.10125 Published online by Cambridge University Press

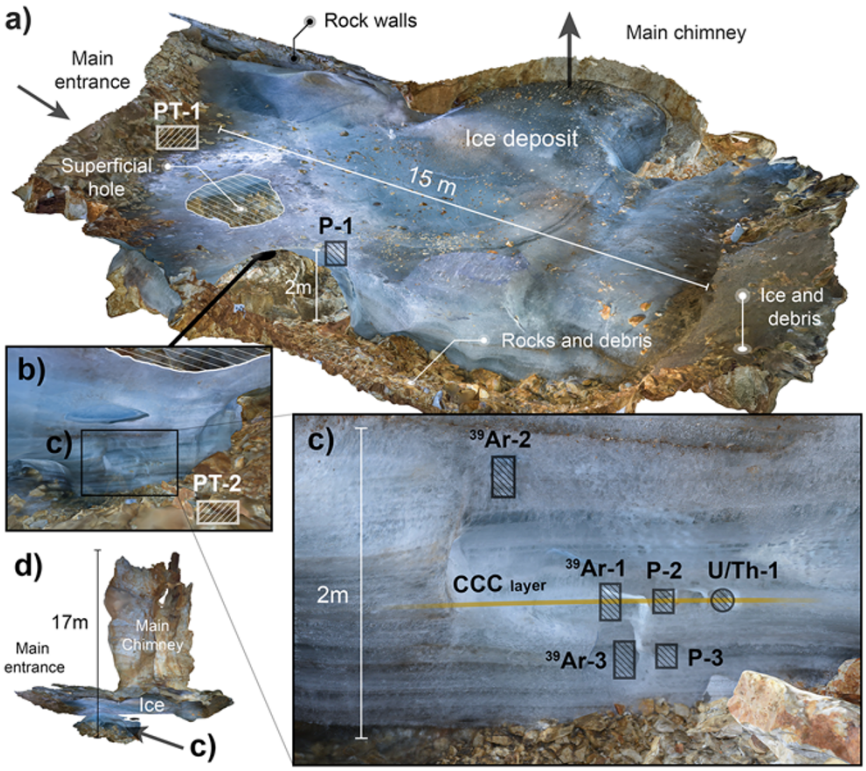

Figure 2. 3D textured mesh of the Leupa ice deposit in November 2021 (a); sampling location at the ice chamber close to the cave bed (b); detail of the sampling location for various dating methods in relation to the CCC layer (c); and Leupa Ice Cave cross-section, including rock walls and main chimney (d). In brown, the position of the CCC layer. The superficial hole formed during summer 2021 was not present at the time of the sampling (Fig. 1c,d). Data from Securo and others (2022b).

calcite (P-2) and (iii) from the base of the ice deposit (P-3) (Fig. 2; Table 2) have been collected for pollen analysis by using a hammer and chisel. Sampling for CCC and ^{14}C dating was carried out on 9 November 2016. Three ice cores were collected using a battery-powered ice corer, each 90 cm in length and 10 cm in diameter. The cores were extracted transversely to the in situ CCC layer. Immediately after extraction, they were carefully placed in plastic bags and stored in a dry ice container for transport to lower altitudes.

3.1. ^{39}Ar dating

The rare noble gas radioisotope ^{39}Ar has a half-life of 268 years (Golovko, 2023). The production of ^{39}Ar takes place in the atmosphere via nuclear reaction of cosmic ray-induced neutrons with ^{40}Ar. Because the atmosphere is the dominant reservoir of Ar in the environment, variations in the production rate lead to relatively minor changes in the atmospheric abundance of ^{39}Ar, which in the past have been assessed to be of little practical relevance for ^{39}Ar dating (Loosli, 1983). A recent reconstruction of past atmospheric ^{39}Ar (Gu and others, 2021), however, inferred variations of atmospheric ^{39}Ar of up to 17%, which are relevant in comparison to the current measurement precision and hence should be taken into account for precise absolute ice dating applications. The very low atmospheric ^{39}Ar abundance (^{39}Ar/Ar $= 7.8{\cdot}10^{-16}$,) and the low solubility of argon in water ($\approx$ 0.4 mL(STP) kg^{-1} of water in equilibrium with air) lead to only $\sim$10 000 ^{39}Ar atoms contained in one kilogram of air-equilibrated water. In ice, Ar is excluded from the crystal structure and resides exclusively in air bubbles (Malone and others, 2010), and the Ar content depends on the formation history of the ice (Utting and others, 2016).

Glacier ice formed from compaction of snow can contain as much as $\sim$100 mL of air per kg (e.g., Buizert and others, 2014) and hence up to $\sim$1 mL of Ar per kg. In various forms of ground ice, the Ar content was found to vary between $\sim$0.1 and 0.5 mL kg^{-1} (Utting and others, 2016). The range of 0.1 to 1 mL kg^{-1} of Ar corresponds to roughly 2000–20 000 ^{39}Ar atoms contained in the enclosed air bubbles of one kilogram of modern ice. Consequently, quantitative detection of ^{39}Ar is extremely challenging and classical analysis by low-level decay counting demands sample sizes in the order of tons (Loosli, 1983). Recently, the adaptation of the ATTA to ^{39}Ar, also called Argon Trap Trace Analysis (ArTTA), has achieved a decisive reduction in the required sample size to a few kilograms of ice (Feng and others, 2019). The ArTTA technique utilizes the isotopic shift in electronic transition frequencies to slow down single ^{39}Ar atoms by laser cooling. The required multi-photon scattering for this process yields perfect selectivity. The ^{39}Ar atoms are captured in a magneto-optical trap and counted using the fluorescence light imaged onto a CCD camera and a fibre connected to an avalanche photodiode. Based on the breakthrough using the ArTTA technique, glacier ice dating by ^{39}Ar has finally become feasible and can now be extended to ice dating applications at various cryospheric archives.

The chain-saw extracted ice blocks (^{39}Ar-1, ^{39}Ar-2 and ^{39}Ar-3) were transported by freezer transport to a −20°C cold room at Heidelberg University. Prior to the argon extraction, the ice blocks were cleaned by cutting off the outermost layers using a bandsaw. The ice blocks were then put into a stainless steel container, which was evacuated with a turbo molecular pump. The entrapped gas was extracted by melting the ice, followed by the transfer of the gas onto a liquid nitrogen-cooled activated charcoal trap via a water trap to remove water vapour. Further gas extraction and purification were performed using the dedicated argon purification system described by Feng and others (2019). It uses a titanium sponge getter at 900°C to remove all gases except for noble gases and hydrogen. A second titanium sponge getter at room temperature

https://doi.org/10.1017/jog.2026.10125 Published online by Cambridge University Press

is used to adsorb hydrogen. The remaining gas fraction consists of >99 % argon, is captured on a charcoal trap and then transported to the ArTTA setup. Further details regarding the ArTTA laboratory and its application to date glacier ice have been described in Feng and others (2019).

3.2. Pollen analyses

The three extracted ice blocks (P-1, P-2 and P-3) have been decontaminated in the lab by surface scrapping and washing with double-distilled water. The ice blocks were then left melting at room temperature in a closed container, and their volume was measured. The so-obtained liquid samples were filtered with a 150 μm mesh size filter to remove possible bedrock fragments. The <150 μm fraction was then filtered with a 7 μm mesh size filter to concentrate the pollen, and this >7 μm fraction was transferred to a 10 mL test tube for chemical treatment. Only highly pointed test tubes were used to avoid the loss of pollen during the chemical treatment (Festi and others, 2019), which consisted of HCl 10% and acetolysis solution (Erdtman, 1960). To gain information about the current pollen flux in the cave, we placed two pollen traps for about a year (August 2017–July 2018). The traps consisted of plastic boxes of 15 × 22 cm (330 cm^2) with the bottom covered in glycerin in order to trap the pollen grains once they fall into the trap. Pollen trap 1 (PT-1) was placed in the cave above the ice deposit at 15 m from the entrance, and trap 2 (PT-2) was placed 'below the ice' next to the location where the ice blocks were cut out of the deposit. The chemical treatment consisted of HCl 10% and acetolysis solution (Erdtman, 1960). In addition, we collected and analysed the pollen content of two moss cushions (PM-1 and PM-2) growing at the entrance of the cave. Mosses are commonly used as modern analogues as they are ideal pollen traps that represent on average a 5 year pollen rain (e.g., Mazier and others, 2009). Chemical treatment followed the standard for fossil pollen analyses (Bennett, 1990). Finally, the pollen content of each ice, moss and pollen-trap sample was mounted in glycerin for identification and quantification. Pollen identification was performed by means of a light microscope at a magnification of 400× and 600×, using the reference collection of the Department of Botany of the University of Innsbruck, in addition to standard identification keys (Moore and others, 1991; Hooghiemstra and others, 2004) and pollen atlas (Reille, 1999). For the ice samples and the pollen trap samples, the complete content of pollen was analysed, while for the mosses, a pollen count of ∼1000 pollen was obtained.

3.3. Cryogenic Cave Carbonates U-Th dating

CCCs form through the segregation of solutes during the freezing of cave ice (Žák and others, 2004, 2008; Dublyansky and others, 2024). Thus, they represent both a proxy for the presence of liquid water as well as for negative cave temperatures.

Five coarse CCC samples were analysed for U and Th concentrations, isotopic ratios and age data using $^{230}Th/^{234}U$ methods. Three samples (LEU-3, LEU-4 and LEU-26) sized 30–42 mg were prepared and analysed at the Trace Metal Isotope Geochemistry Laboratory at the University of Minnesota, USA, while samples (LEU-1 and LEU-2) were prepared and analysed at the Max Planck Institute for Evolutionary Anthropology (EVA), Leipzig, Germany. Prior to analytical chemistry, samples were cleaned ultrasonically in 15 MΩ water for 10 min and leached in a weak 2% HCl solution for 2–3 min to remove surface impurities. Chemical separation and purification procedures were similar to those described in Edwards and others (1987) and Hoffmann and others (2016). Both sets of samples were analysed for U and Th concentrations and isotope ratios using multi-collector inductively coupled plasma mass spectrometry (Thermo Finnigan Neptune or Neptune Plus) using either the measurement protocol described in Shen and others (2012) and Hoffmann and others (2018a). Ages were calculated offline using half-lives from Cheng and others (2013) and are reported relative to 1950 CE with 2-σ uncertainty. The extent of detrital ^{230}Th contamination was examined using $^{230}Th/^{232}Th$ ratios and found to be extremely high, with activity ratios between 0.9 and 1.2, therefore yielding highly unprecise ages when corrected for detrital Th contamination.

Recent work by Töchterle and others (2022) has shown that the construction of isochrons is important for accurate age determination of a patch of CCCs. Given the scattered results in the individual ages, a $^{230}Th/^{238}U$–$^{232}Th/^{238}U$ Osmond A isochron (Ludwig and Titterington, 1994) was constructed in IsoplotR (McIntyre and others, 1966) using the isotopic ratios from the five samples. The mean square of weighted deviations (McIntyre and others, 1966) yields an elevated value of 24, indicating overdispersion in the observed scatter due to non-analytical uncertainties, that is, so-called geological variability (Ludwig and Titterington, 1994). To address this overdispersed data set, we applied the 'Maximum Likelihood with Overdispersion' Model, which attributes the overdispersion in the ages to geological scatter or non-radiogenic isotope composition (Vermeesch, 2018), the latter of which we know to be significant based on the $^{230}Th/^{232}Th$ ratios.

3.4. Ice/water dating ^{14}C

Full details of the method can be found elsewhere (Uglietti and others, 2016; Fang and others, 2021), but are summarized here in brief. Ice samples were transported and kept frozen after collection at PSI until preparation for ^{14}C analysis. Water samples were collected in pre-cleaned flasks (rinsed five times with ultrapure water [UPW]) and kept sealed until treatment. To remove potential contamination of the ice samples, 3 mm of the outer layer was removed with a pre-cleaned stainless-steel bandsaw in a −20°C walk-in cold room. Afterwards, they were rinsed with UPW (18.2 MΩ cm quality) and placed in pre-cleaned 1 L PETG jars (Semadeni; rinsed five times with UPW) for melting. The meltwater (or water from the flasks) was subsequently filtered onto pre-baked quartz fibre filters (Pallflex Tissuquartz 2500QAT-UP). Residual carbonates were removed by triple acidification with 0.5 μL of 0.2 M HCl. All these steps were conducted in a class 100 laminar flow box. At the University of Bern (LARA laboratory), the WIOC filter samples were finally combusted in a thermo-optical OC/EC analyser (Sunset Modeldoc4L, Sunset Laboratory Inc., USA) at 375°C using the Swiss 4S protocol, and ^{14}C measurements of the resulting CO_2 performed online in the 200 kV MICADAS accelerator mass spectrometer (AMS) equipped with a gas ion source and gas interface system. All ^{14}C results are reported as fraction modern (F14C), the $^{14}C/^{12}C$ ratio of the sample divided by that of the 1950-referenced modern standard (NIST oxalic acid II, SRM 4990C), normalized to −25‰ in $\delta^{13}C$. Daily AMS calibration used modern (F14C = 1.3407 ± 0.0005) and fossil (F14C = 0.0018 ± 0.0005) standards. Data postprocessing included correction for cross-contamination in the analytical set-up and for the procedural blank, estimated using artificial ice. Correction for cross-contamination was 0.5 ± 0.4% of the F14C from the previous sample in the measurement sequence, for correction of the constant contamination (background) in the analytical setup C

https://doi.org/10.1017/jog.2026.10125 Published online by Cambridge University Press

Table 1. Results of argon extraction and dating. pmAr denotes 'percent modern argon'. Samples ^{39}Ar-1, ^{39}Ar-2 and ^{39}Ar-3 were taken at locations of the cryogenic cave carbonates (CCC) layer, above and below it, respectively. Error is 1σ.

Block	m from bottom	Weight [kg]	Air [STP mL]	Argon [STP mL]	pmAr	Age corr (Mean/Max/Min) [a b2018]
^{39}Ar-2	1.8	2.8	28.3	0.6	0.77+0.15-0.14	125/205/42
^{39}Ar-1	0.8	6.3	172.2	3.4	0.71+0.11-0.10	157/219/98
^{39}Ar-3	0.4	4.5	95	1.9	0.67+0.16-0.17	178/297/89

mass was 0.4±0.2 μg with a F14C of 0.8±0.36, and the procedural blank accounting for sample preparation and determined from long-term blank monitoring was 1.34 ± 0.62 μg C and 0.69 ± 0.13 for F14C (for ice samples; 0.4± 0.3 μg C for the water samples). These values are within the uncertainty of the previously reported values (e.g., Uglietti and others, 2016; Fang and others, 2021). All uncertainties were fully propagated to the final calibrated ^{14}C ages. ^{14}C calibration was performed in OxCal v4.4.4 (Ramsey, 2021) with IntCal20, the Northern Hemisphere atmospheric calibration curve (Reimer and others, 2020).

4. Results

4.1. Visual ice properties

The ice deposit at the sampling site showed a heterogeneous visual stratigraphy with distinct horizontal layering (Fig. 2c), above a sloped bed. The most prominent feature was an ∼15 cm thick layer of bubble-free ice at ∼170 cm above the bed, separating a homogeneous layer of comparatively lower density and rich in bubbles from the bottommost ice layers. The latter comprised typical glacier-type bubble-rich layers alternating with thinner, cm-thick layers of bubble-free ice. The CCC layer was enclosed in bubble-rich ice at ∼50–70 cm above the bed. It was clearly visible and traceable through its yellow-brown colour.

4.2. ^{39}Ar dating

The results of argon extraction and dating from three ice blocks are shown in Table 1. The blocks comprised between 0.6 and 3.4 mL STP of argon, which is sufficient for ArTTA analysis. A sample size of 1–2 mL Ar is preferred, but as little as 0.5 mL STP has been used successfully (Feng and others, 2019). The inverse correlation between sample weight and relative error (Table 1) is expected in ArTTA analyses. Smaller samples are more strongly affected by the background of ^{39}Ar building up in the circulating gas during the analysis, leading to larger corrections and thus higher relative uncertainties (Feng and others, 2019). In addition to the measured ^{39}Ar contents in percent modern argon (pmAr), which can directly be translated into apparent ages using the decay law, Table 1 also provides corrected ^{39}Ar ages, taking into account the temporally varying atmospheric concentration of ^{39}Ar. The results show age differences among the three dated ice blocks that are not significantly distinguishable in view of their dating uncertainty. The ^{39}Ar content is clearly non-modern, however, and the mean corrected age of the three blocks suggests an age of 153 years before 2018, corresponding to 1865 CE, with an uncertainty of about ±70 years.

4.3. Pollen analyses

Pollen concentration in the ice samples ranges from 185 to 580 pollen L^{-1}, and total counts vary from 738 to 1410 pollen per sample (Supplementary Table 1). The pollen assemblages include up to 50 pollen types, four types of cryptogam spores, one type of fungi spore and two types of testate Amaebae. In addition, a stoma of *Larix* (larch) and microcharcoal particles have been recovered. Arboreal pollen dominates in all three samples, with *Pinus sylvestris/mugo*-type (pine) and *Picea* (spruce) dominating P-1 and P-3, while sample P-2 is characterized by a wide spectrum of thermophilus taxa, like *Ostrya* (hornhop), *Quercus robur*-type (deciduous oak), and *Corylus* (hazel). Table 2 reports the occurrence of the potential Holocene time markers: *Ambrosia* (ragweed), *Zea mays* (maize), *Castanea sativa* (sweet chestnut) and *Juglans regia* (common walnut), and shows that they are present in all three samples, only *Z. mays* is missing in P-2. Modern sample of mosses represent several years of pollen deposition, and their pollen assemblages are characterized by abundant arboreal pollen, especially of *Pinus* and *Picea* similar to P-1, that is, the surface sample. Time markers as *Ambrosia* (ragweed), *Z. mays* (maize), *Castanea sativa* (sweet chestnut) and *J. regia* (common walnut), occur in both samples, except for PM-1, where *Z. mays* is missing. The analyses of the pollen traps resulted in 571 pollen for PT-1, revealing a pollen rain of 19 pollen dm^{-2} a^{-1}. The pollen trap placed below the ice surface (PT-2) accumulated significantly less pollen, for a total of 122 pollen (4 pollen dm^{-2} a^{-1}). In PT-1 *Ambrosia* is absent but *Z. mays* is present along with *C. sativa* and *J. regia*. In the PT-2, below the ice, all four pollen types were absent. According to this occurrence, the most likely maximum age of the Leupa ice samples based on pollen analyses is ∼120 years, namely the beginning of the 20th century, as Ambrosia was first reported in northern Italy in 1902 (Vignolo-Lutati, 1934).

4.4. Cryogenic Cave Carbonates U-Th dating

The CCC analyses reveal a U concentration ranging between 380 and 430 ng g^{-1} and high detrital Th contamination as indicated by ^{230}Th/^{232}Th activity ratios of 0.9–1.2. Correction for detrital Th using the a priori value of 0.8 ± 0.4 derived from silicate bulk earth (Wedepohl, 1995) yields corrected ages with extremely large uncertainties that are indistinguishable from 0. The ^{230}Th/^{238}U–^{232}Th/^{238}U isochron age, which accounts for overdispersion, yields an age of 0.056 ± 68 years, and an initial ^{230}Th/^{232}Th activity ratio of 0.9 ± 0.009, in agreement with the value derived from silicate bulk earth (Wedepohl, 1995). Despite the apparent scatter initially observed in the individual ages, the isochron plot (Fig. 3) suggests that the CCCs likely formed from the same parent solution during a single freezing event. Within the uncertainty, it can be assumed that CCCs formed in the last decades of the last century.

4.5. ^{14}C dating of cave ice and water samples

Radiocarbon (^{14}C) dating of the WIOC fraction was performed on two ice samples. Both samples yielded sufficient carbon mass for ^{14}C AMS analysis and dating (61 and 36 μg C). They resulted in consistent and closely matching calibrated ages with a σ range of 2760–2430 and 2950–2500 years cal BP, respectively (Fig. 4). There

https://doi.org/10.1017/jog.2026.10125 Published online by Cambridge University Press

Table 2. Occurrence of pollen time markers in the ice samples (P-), modern moss samples (PM-) and in cave pollen traps (PT-). CCC is cryogenic cave carbonates.

Sample code	Maximal age indicated by marker	P-1	P-2	P-3	PM-1	PM-2	PT-1	PT-2
Position		Surface of ice	CCC layer in the ice	Base of the ice	Cave entrance	Cave entrance	In cave above ice	In cave below ice
Volume [l]		2.43	2.12	3.99	-	-	-	-
Ambrosia	1900 CE	10	14	1	3	15	-	-
Z.mays	1493 CE	5	-	1	-	1	2	-
C.sativa	800 BCE	1	10	9	7	17	2	-
J.regia	800 BCE	3	5	1	2	1	3	-

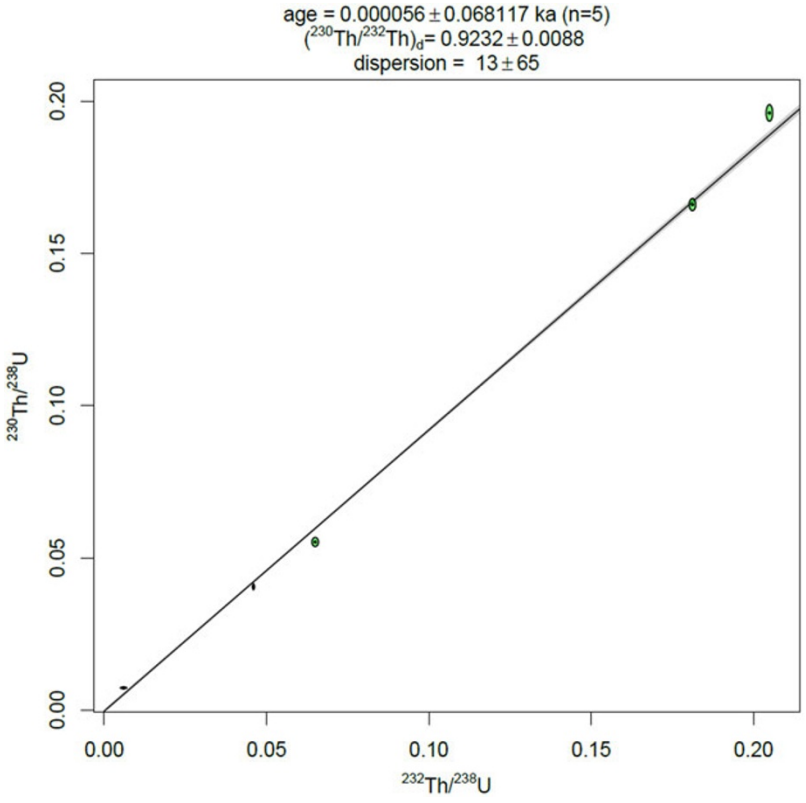

Figure 3. $^{230}Th/^{238}U$–$^{232}Th/^{238}U$ isochron derived from five LEU CCC samples using IsoplotR (Vermeesch, 2018).

seems to be no bias due to the higher calcite amounts present in the cave. There was sufficient organic carbon in the samples.

For the modern water samples collected during Summer 2017, only one sample (LEUPA-water-2) yielded a sufficient mass of 18 μg C to allow ^{14}C dating (Fig. 4). The available C mass for AMS analysis from LEUPA-water-1 was 3.4 μg, significantly less than the recommended amount of 10 μg for this method, as indicated by the large uncertainty (Uglietti and others, 2016; Dyonisius and Jenk, 2025). However, we note that within the uncertainty, the result was consistent with LEUPA-water-2 in terms of its F14C (and $\delta^{13}C$). The one sigma range of the calibrated age for the successful sample (LEUPA-water-1) was 1280–920 years cal BP, suggesting that the contemporary drip water carries pre-aged organic carbon. The $\delta^{13}C$ values of all samples (ice and water) ranged between −22 and −27 per mil, which is the typical for range for biogenic organic material (between around −20 to −30 per mil). This indicates no contribution from remains of carbonate (typically ∼0 per mil in $\delta^{13}C$), as expected due to the removal procedure during sample preparation (and the relatively low combustion temperature applied) prior to ^{14}C analysis. A significant age bias related to input from limestone carbonate in the karst system can thus be excluded.

5. Discussion

The possibility to employ four different state-of-the-art ice dating methods at a single location represents a novelty and a unique opportunity, which we have taken advantage of in this study. This is particularly relevant for ^{39}Ar dating, which has never been applied before to cave ice, as well as for the presence of pollen and a CCC layer, which may enable U-Th dating, and the radiocarbon (^{14}C) dating of the WIOC fraction. Although the Leupa Ice Cave is an exceptional case in this respect, the relevance of our findings regarding methodological aspects in cave ice dating extends beyond this particular location. Accordingly, we discuss the implications of each dating method individually but give special attention to possible consistent interpretations drawn from their joint evaluation.

With regard to ^{39}Ar-dating, a special challenge arising from cave ice could have concerned the limited air content, depending on the ice formation history, for example, if ice is formed by refreezing meltwater. At Leupa, we found sufficient bubble-rich layers in the stratigraphy for sampling. The air, and thus argon, content of each of the three analysed blocks was sufficient for reliable measurements and counting statistics, even though it was considerably

https://doi.org/10.1017/jog.2026.10125 Published online by Cambridge University Press

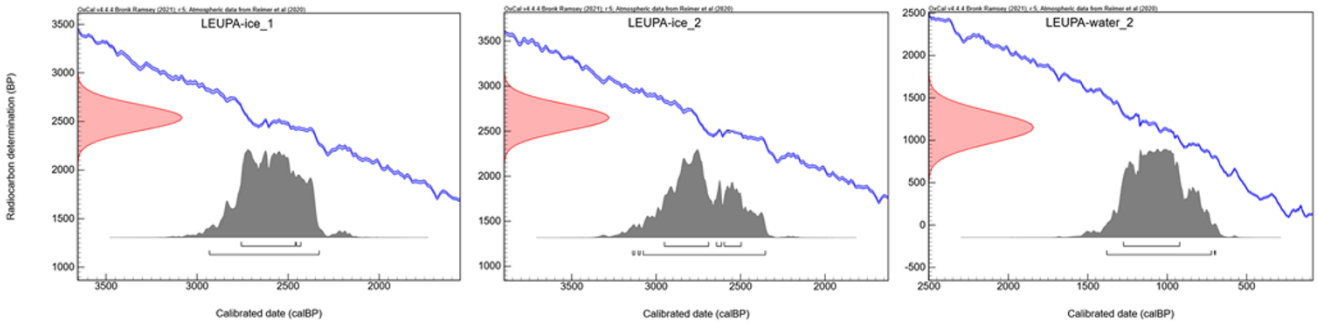

Figure 4. ^{14}C calibration of the WIOC ice and water samples from the Leupa Ice Cave. Determined radiocarbon age (red; shown as a Gaussian probability distribution corresponding to the determined overall analytical uncertainty) and final calibrated ^{14}C age probability distributions in grey as derived in OxCal v4.4.4 (Ramsey, 2021), using the IntCal 20 radiocarbon calibration curve (blue;). The bars below the probability distribution (grey areas) indicate the one and two sigma age range, respectively. Figure adapted from plots in OxCal.

Table 3. Radiocarbon (^{14}C) results based on the WIOC fraction in the LEUPA samples (ice and water), given as F14C, ^{14}C ages and calibrated ^{14}C ages. Numbers of the carbon amount available for ^{14}C AMS analysis are also provided. Note that BP refers to the year 1950 CE. Ice samples have been analysed on 20 April 2017; water samples have been analysed on 20 February 2020.

Sample	AMS Lab nr	Sample mass, water or ice [kg]	Mass for AMS analysis [μg C]	F14C	^{14}C age [a BP]	^{14}C age 1σ range [a BP]	^{14}C age 2σ range [a BP]
LEUPA-ice-1	BE-7012.1.1	439	61.3	0.729±0.012	2539±132	2757–2430	2932–2330
LEUPA-ice-4	BE-7014.1.1	463	35.8	0.719±0.013	2650±145	2951–2497	3139–2353
LEUPA-water-1	BE-12747.1.1	809	3.4	0.803±0.090	1763±926	n/d	n/d
LEUPA-water-2	BE-12746.1.1	1496	18.0	0.867±0.020	1151±182	1276–922	1381–698

lower than typical values for glacier ice formed by the compaction of snow. The air and argon contents of sample ^{39}Ar-3 were consistent with expectations for air-equilibrated water, whereas the gas contents of samples ^{39}Ar-2 and ^{39}Ar-1 were lower and higher, respectively (Table 1). This suggests the influence of counteracting processes affecting air content, such as partial melting leading to gas loss, or surface micro-structures (e.g., due to hoarfrost formation) leading to air inclusions. In any case, it is likely that gas inclusion occurred contemporaneously with ice formation; hence, no age difference between the ice and the gas, as observed in ice sheets with thick firn layers, is expected. The uncertainty associated with the ^{39}Ar dating mainly corresponds to the statistical counting error, and is of the order of 40–60% of the derived ages. Although the uncertainty does not allow to infer an age gradient among the three samples, the ^{39}Ar values are clearly non-modern, with best estimates ranging from 125 to 178 years from 2019 AD (Table 1). In this sense, this study has presented the first evidence of feasibility to date ice from an ice cave using the ArTTA method. Of particular relevance for ice caves, ^{39}Ar is not prone to contamination from organic soil material, as it relies on the atmospheric air trapped at the time of ice formation.

The mean pollen and spores concentration in the Leupa ice samples (∼434 298 pollen and spores L^{-1}), as might be expected, is significantly lower than values known for glaciers in the Eastern Alps, where mean concentrations are ∼25-28 000 pollen and spores L^{-1} (Festi and others,). This is clearly caused by the fact that pollen input in the cave relies on cave ventilation conditions. Specific pollen types like those produced by *Ambrosia artemisifolia L.* (ragweed), *Z. mays L.* (maize), *C. sativa Mill.* (sweet chestnut) and *J. regia L.* (common walnut) are relevant time marker for the Holocene, as we know when these plant species were first introduced in the European continent and/or when they were spread in the region for cultivation. Ragweed was accidentally introduced as a seed contaminant in Europe at the beginning of the 20th century, and it is currently problematic, especially for its high allergenic pollen (Bonini and Ceriotti, 2020). The first reported specimen in Italy was described in 1902 in the north-west region of Piedmont (Vignolo-Lutati, 1934). Maize was introduced in Europe following the arrival of Europeans in America in 1492. Historical sources indicate that in Italy, despite it had been imported immediately after 1492, it became a common crop only during the second half of the 1500s (Brandolini, 2009). Sweet chestnut and common walnut were cultivated in the Mediterranean since the Classical Antiquity (800 cal BCE) and were spread by the Romans (Mercuri and others, 2013). Their first occurrence in pollen diagrams of the Po Plain (South of the Alps) is in fact dated to the beginning of the Iron Age (Ravazzi and others, 2011), while in diagrams from the south-eastern Alps the first sporadic occurrence is dated around 0 CE (Festi and others, 2015; Segnana and others, 2020). Pollen assemblages from the ice samples all contain ragweed pollen, the most recent of the time markers, which was introduced at the beginning of the 20th century. According to this occurrence, the most likely maximum age of the Leupa ice samples based on pollen analyses is ∼120 years, namely the beginning of the 20th century.

U-Th dating of the CCCs was hindered by high levels of detrital ^{230}Th contamination, as appears to be typical for fine-grained CCC (Spötl and Koltai, 2025), leading to large age uncertainties. Isochron analysis suggests that the CCCs likely formed during a single freezing event, as indicated by their occurrence in a distinct layer of the ice. The best estimate of the isochron age is zero (i.e., corresponding to the year 2017) and considering the associated uncertainty, this implies a formation age from 1949 onward. The CCC was found in situ in November 2015 within a vertical ice outcrop at ∼0.8 m from the bottom of the deposit, and was sampled in November 2016 (Colucci and others, 2017b). Furthermore, the first direct observation of ice in the Leupa Ice Cave dates back to the 1970s (Mikolic, 1979), providing a minimum age constraint of at least 50 years. The cartographic survey produced at that time already documented an ice deposit with geometry and volume broadly similar to, if not greater than, those observed in the 2000s.

https://doi.org/10.1017/jog.2026.10125 Published online by Cambridge University Press

Still, the question remains whether the CCCs could be younger than the surrounding ice. It should be noted that CCC results from the freezing of water on or within ice and is influenced by climate, cave hydrology and microclimate (Žak et al., 2018). The formation of CCC within ice (as opposed to on top of it) is a rare but well-documented process in some glaciokarst environments (e.g.,). The process involves the precipitation of calcite from aqueous solutions undergoing partial freezing inside the ice body. Water saturated or supersaturated with calcium bicarbonate, typically of karstic origin, infiltrates or becomes trapped within the ice, for example, through cracks, pores, or conduits in the ice. As temperatures drop below 0°C, the water begins to freeze. The forming ice crystals consist mainly of pure H_2O and therefore exclude dissolved ions, such as Ca^{2+} (Žák and others, 2012). This exclusion causes a progressive concentration of solutes in the remaining unfrozen liquid. Due to the increasing ionic concentration and the temperature drop, the solution becomes supersaturated with respect to calcite, leading to its precipitation. This process is favoured by the decreasing solubility of calcite at low temperatures, CO_2 degassing (if present in micro-bubbles) and slow ion diffusion in the confined liquid.

Eventually, calcite precipitates within micro-voids, channels, or inclusion pockets inside the ice, forming CCC, as the one recovered from Leupa Ice Cave. Stable isotope analyses ($n = 4$) conducted in 2016 on two crystal aggregates yielded $\delta^{13}C$ values ranging from 6.6‰ to 6.9‰ and $\delta^{18}O$ values between −12.0‰ and −11.8‰ (Colucci and others, 2017b). While somewhat enriched relative to typical CCC-coarse values, these isotopic signatures closely resemble those of certain aggregates reported, for example, from Mitterschneidkar Eishöhle Cave (Spötl and Cheng, 2014).

On the other hand, fine-grained CCCs are commonly observed in modern ice caves and form in the heterothermic zones (Luetscher and Jeannin, 2004) where diurnal and seasonal temperate cycles are well expressed and advective air flow and seasonal freezing dominate the cooling process. The CCC crystals found in Leupa Ice Cave are located precisely in this section of the cave. On the contrary, coarser CCC might form in subaqueous settings (i.e., pools in ice), allowing for very slow freezing and prolonged crystal growth, as evidenced by their much larger size compared to fine-grained CCC, and much lower stable isotopic composition. Recent studies raise questions about the dichotomy of the two classes of CCC and suggest a more complex interplay between the fine and coarse CCC formation mechanisms (Spötl and Koltai, 2025).

In the Leupa Ice Cave, there was the fortunate opportunity to observe, between summer 2020 and 2022, the birth and growth of CCC in statu nascendi, both on the surface of the ice and within small pools embedded in the ice (Figs. 2a and 5b,c). A similar observation was recently, for example, documented in the Winter Wonderland Cave, USA (Munroe and others, 2021). Moreover, morphological evidence observed in the ice suggests that the formation of voids within the ice, where liquid environments favourable to CCC crystal formation can develop, appears to be a common process. In Fig. 2b, just above the sampling area shown in panel c and in Fig. 5d, an intra-ice cavity is visible. Figure 5a,b documents the evolution of another void within the ice, emerged during summer 2020 from the rapidly melting ice. The amount of CCC crystals observed within the water pool in the emerging void during autumn 2020 appears to be lower than that observed the following year (Fig. 5b, 2020, 2021), when the superficial hole formed, with raft-like crystal aggregates exceeding 1 cm (Fig. 5c).

Based on this evidence, and solely from visual observation, these voids seem to develop within ice layers with distinct characteristics, possibly related to different phases of ice accumulation. These layers may serve as discontinuity surfaces, along which thin water films can infiltrate, gradually leading to the radial widening of small intra-ice voids and eventually creating protected micro-environments conducive to the growth of CCC crystals.

The results obtained from the dating of cryogenic calcite, which suffer from large uncertainties due to high thorium contamination, together with the considerations discussed above, lead us to propose two possible scenarios that could account for this result. (i) The CCC layer may have formed from water freezing on the surface of the ice (possibly during a milder phase), at a time when the topographic surface of the ice was lower, and therefore the dated material might actually reflect the age of the ice itself. To justify this result, given that the 2σ uncertainty is 68 years, which might fall within the range of the pollen dating, we would have to assume a 4σ uncertainty (136 years) to be consistent with the ^{39}Ar results. (ii) The CCC may have formed within a void inside the ice, at a time subsequent to the accumulation phase of the deposit, and therefore does not necessarily reflect the timing of ice accretion.

Radiocarbon (^{14}C) dating of the WIOC fraction, performed on the same ice core layer where CCC, pollen and ^{39}Ar dating were applied, shows clear disagreement with these independent methods, all of which indicate a significantly younger age. To investigate this discrepancy, we collected modern drip water, that is, the water presumed to be the source of ice accumulation in the cave, and analysed its WIOC content for ^{14}C dating. The modern water yielded a calibrated age range of 740–1180 cal BP (1σ), indicating that even contemporary drip water transports pre-aged organic carbon. These results reveal that the WIOC fraction in this context does not record the timing of ice formation, but instead reflects the age of carbon mobilized within the karst system, likely derived from aged soil reservoirs. While the water source itself is likely consistent, the distribution and origin of organic matter in the cave environment may vary with flow paths and seasonal dynamics, as shown by Rowan and others (2024).

The reservoir age may not be the only explanation for the radiocarbon results. After around 1850 CE, radiocarbon analysis of ice cores clearly shows a significant and often rapid increase in both organic and elemental fossil carbon concentrations, directly reflecting the impact of industrialization and fossil fuel combustion on atmospheric composition (Jenk and others, 2006). As a consequence, the WIOC fraction includes carbon derived from fossil fuel sources, which are ^{14}C-dead (i.e., it contains no radiocarbon), and thus artificially lowers the ^{14}C content of the sample, making it appear significantly older than it really is. This introduces an inbuilt age. This means that the ^{14}C measured in WIOC from samples younger than around 1800–50 CE no longer reflects the contemporary atmospheric ^{14}C at the time of deposition. As a result, samples younger than ∼200 years cannot be reliably dated with this method, as fossil carbon causes a systematic age bias toward older ages (Jenk and others, 2006). To correct this bias, one would need to account for the fraction of fossil-derived carbon. However, this is difficult due to the lack of precise data on the proportion and variability of fossil carbon inputs over time and space. This uncertainty is illustrated in the same study where a not fully understood dip in F14C is observed between 1870 and 1900. A reasonable estimate for the fraction of modern (non-fossil) carbon in ice during the late 1800s is ∼80% (F14C 0.8, where 1 corresponds to 1950). This estimate is consistent with what has been measured

https://doi.org/10.1017/jog.2026.10125 Published online by Cambridge University Press

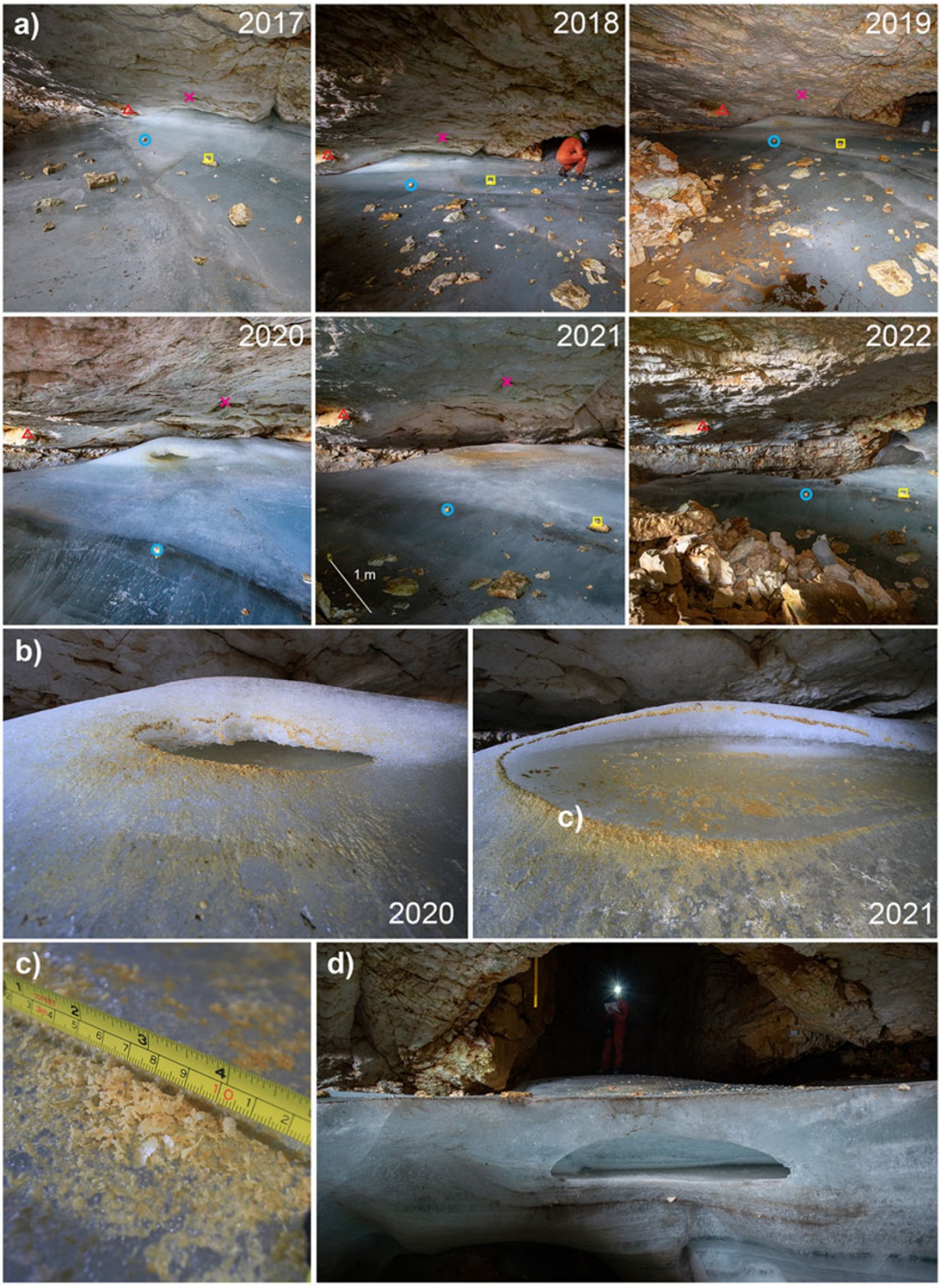

Figure 5. CCC observed in statu nascendi in 2017–22 inside Leupa Ice Cave (a); overview of the main area of CCC formation in 2020 and 2021 (b); detail of CCC crystals (c); and another sector of Leupa Ice Cave where an intra-ice void with a small water pond was observed (d).

in the Leupa samples (Table 3), further supporting the interpretation that these samples likely contain a significant fossil carbon component, and therefore might not be reliably dated using ^{14}C of WIOC.

In summary, while this dating method has proven highly robust and reliable for glacier ice, where the WIOC fraction reflects the bulk of the incorporated ice and represents an insoluble carbonaceous aerosol fraction with a potential inbuilt age of significantly <100 years (Fang and others, 2021), it should be applied with care for the dating of cave ice, especially if likely formed mostly from dripping water. To our knowledge, this has nowhere been discussed before and represents an additional contribution of this study. Collectively, these results highlight the importance of integrating multiple, independent dating methods to obtain more robust chronologies for cave ice deposits.

https://doi.org/10.1017/jog.2026.10125 Published online by Cambridge University Press

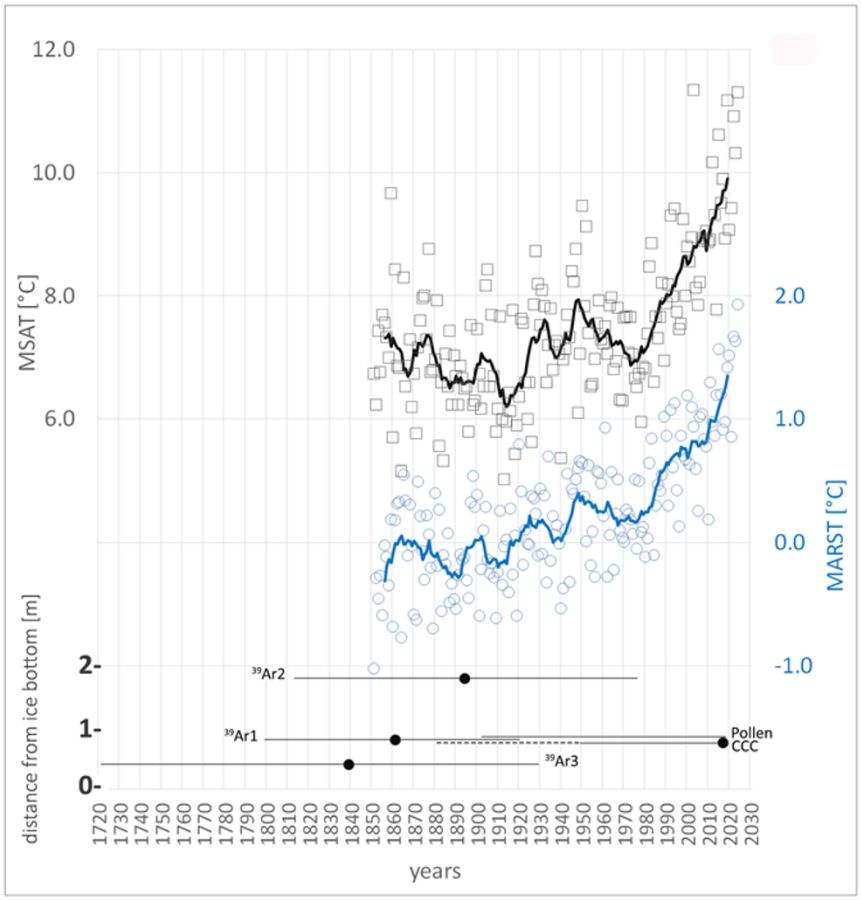

Figure 6. Eleven-year moving average (bold lines) of mean summer air temperature (MSAT) (Colucci and Guglielmin, 2015) and mean annual rock surface temperature (MARST) (Colucci and Guglielmin, 2019). Below; Pollen, ^{39}Ar and CCC dating intervals with distance from ice bottom (m). The solid line is respectively 1σ error for ^{39}Ar and 2σ error for CCC. 4σ error for CCC is the dashed line.

Given all these considerations, both the pollen and CCC data (adopting scenario i) above) can only constrain the maximum age of the respective section of the ice column to approximately the beginning of the 20th century. The ^{39}Ar data provide age constraints in both directions and, in addition to covering the depths of the CCC layer (^{39}Ar-1; Fig. 2) and the pollen samples (^{39}Ar-3; Fig. 2), also include a sampling point located higher up in the ice stratigraphy (^{39}Ar-2; Fig. 2). The range of the three mean ^{39}Ar ages between 125 and 178 years before 2019 indicates a formation time between 1840 and 1893, at the end of the main phase of the LIA (1575–1860;), but slightly older than expected from the other age indicators. However, a formation in 1920 would also be consistent with all ^{39}Ar data points within 1σ uncertainties. Overall, the early 1900s appear to be the most likely formation period, fully consistent with the pollen constraint, in agreement with the ^{39}Ar ages within 1σ uncertainties and with the younger CCC isochron age or taking into consideration the alternative CCC deposition inside the ice block.

This finding argues against the ice being substantially older at the very base of the ice deposit, further suggesting that all the ice column formed rather fast. Even though a direct correlation between external glaciation and cave glaciation is not always possible, and can often lead to misleading interpretations, in a broader context looking beyond the microclimate of the Leupa Ice Cave, the rapid growth of the cave ice body would tie well with the latest phase of climatic conditions favourable for glacier growth known at the end of the LIA, in the Julian Alps (Colucci, 2016). In this regard, evidence shows how between 1910 and 1920 a positive phase for the mass balance of glaciers occurred in the Julian Alps (Colucci and Žebre, 2016), capable of geomorphologically reshaping the terminal Holocene moraines in the area (Colucci, 2016).

The maximum age deduced from the ^{39}Ar ages is chronologically consistent with the peak of the LIA in the Alps, between 1780 CE and 1860 CE (Nicolussi and others, 2022). More specifically, in the Eastern Alps at Pasterze glacier (Carinthia, Austria), the LIA peak is dated back to 1855 CE (Nicolussi and Patzelt, 2000). Nevertheless, it is worth remembering that cave ice formation, such as in the Leupa Ice Cave, requires infiltrating water and reflects more a local permafrost dynamic than a lowering of the Equilibrium Line Altitude, which is primarily associated with decreasing summer temperatures (Žebre and others, 2021). In this sense, comparing our results with the chronology established by Racine and others (2022), based on eight sag-type ice caves, may yield contrasting outcomes due to the different geometry and modes of ice formation and accumulation. Nevertheless, the cave closest to Leupa (Großer Naturschacht), located in South Tyrol, shows that the upper 10 m of the deposit accumulated at an average rate of 5.4 cm w.e. yr^{-1}. In any case, the results consistently indicate that the LIA represents the most significant Holocene period of positive mass balance even for ice deposits in sag-type caves.

The pollen and CCC constraints suggest that the ice in Leupa Ice Cave did not form at the peak of the LIA, but rather in the early 20th century. While the cold climate of the LIA peak resulted in maximum glacier advances, it may have been too cold to support ice formation in the cave under permafrost conditions (Žák and others, 2012). In this situation, the mean mass balance of

https://doi.org/10.1017/jog.2026.10125 Published online by Cambridge University Press

Figure 7. View from the main entrance of the Leupa Ice Cave ice deposit, the day of the pollen and ^{39}Ar sampling on 3 October 2018 (a) and on 8 November 2024 during a more recent fieldwork (b). Vertical white bars in (b) show the location of the 2016 and 2018 sampling.

the ice deposit may have been negative due to sublimation effects induced by active ventilation of the cave's heterothermic zone. Slightly warmer conditions, however, may have facilitated the presence of infiltrating water in the cave during summer, while still being cold enough to freeze large quantities of this water, leading to a rapid buildup of the ice mass.

The oldest available temperature climatology from the area, recorded 2 km west at 2200 m a.s.l., belongs to the 30 year period 1851–80 CE. Applying a normal lapse rate of 0.0065°Cm^{-1}, MAAT at the elevation of the cave entrance (2300 m a.s.l.) was equal to −0.8°C (σ = 0.8), while the mean annual rock surface temperature (MARST) in the Leupa Ice Cave was reconstructed to −0.6°C (Colucci and Guglielmin, 2019) (Fig. 6). This value is consistent with the hypothesis that the rock walls of the cavity were in permafrost conditions.

Since MARST is closely related to MAAT, we have also included the mean summer air temperature (MSAT; Jun–Jul–Aug) in Fig. 6, as it has a greater influence on the glacier ablation period. It shows that MSAT tended to decrease until around 1920, after which it rose rapidly. At the same time, the particularly warm summer of 1859 stands out. MARST remained relatively stable at slightly below 0°C during this period. Nevertheless, milder phases occurred between 1860 and 1870 and around the turn of the 20th century. From 1920 onward, MARST gradually began to rise and, since the 1980s, has not dropped below the 0°C threshold.

More recently, the ice deposit in Leupa Ice Cave has been rapidly melting since 2014 (Fig. 6), which is the year when evidence points to the complete degradation of permafrost in the rock walls (Colucci and Guglielmin, 2019). Specifically, incoming milder air flows are generating a significant effect, particularly through the debris at the base of the ice. This process leads to the initial widening and subsequent disappearance of a dome-shaped melting cavity beneath the ice body (Figs. 1c,d and 7). This ephemeral cavity beneath the ice has been present since the early explorations of Leupa Ice Cave in the 1970s (Mikolic, 1979). At that time, climatic conditions were generally favourable to glaciation, also outside the cave. In the Alps overall, and specifically in the Julian Alps, this period corresponds to the last recorded phase of glacial advance (Colucci and Guglielmin, 2015), during which permafrost conditions likely existed at the elevation of Leupa Ice Cave (Colucci and Guglielmin, 2019). These latter considerations may alternatively explain why no older ice is found at the base of the deposit. The presence of pronounced warm airflow through the debris beneath the ice likely contributes to the continuous, albeit slowed, melting of its basal layers. In this context, a dynamically ventilated and active cave like Leupa (Securo and others, 2022b), with multiple entrances located at different elevations, reasonably supports the assumption of a particularly significant mass turnover. Periods of rapid deposit growth under favourable conditions stand in sharp contrast to gradual reductions during climatically unfavourable periods, which are further exacerbated by air flow feedback. As emphasized by Securo and others (2022b), since water dripping is the primary source of ice accretion, ice losses in the caves of the area are generally more pronounced where snow ingress and firnification processes are inhibited by the cave's geometry. The recent climatic evolution, marked by the rapid increase in average air temperatures, is rapidly degrading the underground cryosphere of the Alps, with the dramatic consequence of losing the palaeoclimatic information contained inside the ice.

6. Conclusion

This study presents a novel dating of a permanent ice deposit in the Leupa Ice Cave (Julian Alps) using, for the first time, ^{39}Ar dating via ArTTA, and combining the results with three independent methods: pollen analysis and U-Th dating of CCC and the WIOC via ^{14}C. The concurrent application of these methods has proven not only technically feasible but also complementary, allowing for a robust chronological reconstruction despite inherent limitations of each proxy.

The successful use of ^{39}Ar dating represents a breakthrough in cave ice studies, demonstrating that even low-air-content ice can yield reliable results when ice layers with sufficient air bubbles are present. The ^{39}Ar results consistently point to ice formation between 1840 and 1893 CE, placing the origin of the deposit in the late phase of the LIA, or right at the onset of the post-LIA climate amelioration phase. Though not necessarily causally connected, this is in agreement with the broader climatic framework of the Eastern Alps, which experienced the onset of glacier retreat and the gradual increase in summer temperatures starting from the 1920s onward.

Pollen analysis, although limited by expected low concentrations, identified key time markers such as *Ambrosia artemisiifolia* and *Z. mays*, constraining the maximum age of the ice to the early 20th century. CCC dating, affected by detrital thorium contamination, yielded younger and less precise ages. However, considering the alternative interpretation of intra-ice deposition, these results remain broadly consistent with the ^{39}Ar and pollen data.

https://doi.org/10.1017/jog.2026.10125 Published online by Cambridge University Press

Taken together, the three dating methods indicate that the ice in Leupa Ice Cave most likely formed rapidly during a relatively short time window between the late 19th and early 20th century, a period marked by climatic conditions capable of sustaining both permafrost and episodic meltwater inflow necessary for ice accumulation. The combined stratigraphic and chronological evidence suggests that the entire ice body may have formed in response to these conditions, rather than gradually over centuries. The absence of older ice layers at the base of the deposit, as might be expected, may be explained by an effective mass turnover, possibly driven by intermittent inflows of milder air from below, which likely sustained continuous melting over time, as well as by sublimation processes in a ventilated cave environment such as Leupa. Our findings also emphasize that in karst environments, caution is needed when interpreting WIOC ^{14}C ages for dating of cave ice. A systematic bias toward older ages due to the reservoir effect from aged ^{14}C in the soil/karst is very likely to exist. Moreover, in this specific case of Leupa samples, the ice is too young for reliable ^{14}C dating using WIOC, due to the effect of inbuilt age from fossil-derived carbon.

This research highlights the importance of integrating different dating techniques in cave ice studies, particularly when individual proxies are affected by environmental or methodological uncertainties. Our findings emphasize the potential of ^{39}Ar dating as a powerful new tool for ice in caves, and provide a framework for future studies. This aspect is of particular relevance and urgency, as the current phase of rapid warming is quickly degrading these important underground palaeoclimatic archives.

Supplementary material. The supplementary material for this article can be found at https://doi.org/10.1017/jog.2026.10125.

Acknowledgements. This work was carried out within the C3 project, Caves Cryosphere and Climate, sponsored by the *Società Alpina delle Giulie* through its speleological group *Commissione Grotte Eugenio Boegan*, and realized in the framework of the cooperation agreement named 'Accordo di collaborazione scientifica nei settori della climatologia, meteorologia, geologia, carsismo, glaciologia e divulgazione scientifica' Prot. ISMAR n. 0001035 of 08-02-2017 promoted with the Marine Science Institute of the National Research Council (ISMAR-CNR). PB gratefully acknowledges funding by the Austrian Science Fund (FWF; grant no. I 5246-N). The development and application of ArTTA has been funded by several grants of the German Science Foundation (DFG), relevant for this work are DFG grants AE 93/17-1, OB 164/12-1, AE 93/22-1 and OB 164/17-1. Arne Kersting, Zhongyi Feng, Lisa Ringena, Max Schmidt and Julian Robertz contributed to ^{39}Ar sample preparation, analysis and data evaluation. DLH acknowledges Max Planck Society / MPI Eva for U-Th analysis. We acknowledge the Civil Defense of Friuli Venezia Giulia for the long-term logistic support during fieldwork activities.

Author contributions. Coordination: RRC; Conceptualization: RRC, ML, PB, DF; Methodology: RRC, ML, PB, DF, WA, GEM, DW, MS; Formal analysis ^{39}Ar: WA, DW, SM; Formal analysis pollen: DF; Formal analysis U-Th: ML, DLH, GEM, RLE; Formal analysis ^{14}C: MS, TMJ, AE; Visualization: RRC, AS, TMJ; Writing—original draft: RRC, WA, ML, PB, DF, AS; Writing—review & editing: all authors.

References

Adhikari P and 9 others (2023) Precision measurement of the specific activity of 39Ar in atmospheric argon with the deap-3600 detector. *The European Physical Journal C* **83**(7), 642.

Bennett K (1990) Review of textbook of pollen analysis, by K. Faegri, J. Iversen (4th edition revised by K. Faegri, P.E. Kaland, K. Krzywinski). Chichester: John Wiley and Sons, 328 pp.

Bertozzi B, Pulvirenti B, Colucci RR and Di Sabatino S (2019) On the interactions between airflow and ice melting in ice caves: A novel methodology based on computational fluid dynamics modeling. *Science of the Total Environment* **669**, 322–332.

Bonini M and Ceriotti V (2020) Ragweed story: from the plant to the patient. *Aerobiologia* **36**(1), 45–48.

Borsato A, Miorandi R and Flora O (2004) I depositi di ghiaccio ipogei della Grotta dello Specchio e del Castelletto di Mezzo (Dolomiti di Brenta, Trentino): morfologia, età ed evoluzione recente. *Studi Trentini di Scienze Naturali, Acta Geologica* **81**, 53–74.

Brandolini A (2009) Maize introduction, evolution and diffusion in Italy. *Maydica* **54**(2), 233.

Brevini F, Bianchi G, Conti L, De Marchi M and Esposito R (2004) *Rocce: dal Borneo alle Lofoten, dalle Alpi al Sahara: avventure di uomini in scalata.* Mondadori: Milano, 252.

Buizert C and 9 others (2014) Radiometric 81Kr dating identifies 120,000-year-old ice at Taylor Glacier, Antarctica. *Proceedings of the National Academy of Sciences* **111**(19), 6876–6881.

Cheng H and 9 others (2013) Improvements in 230Th dating, 230Th and 234U half-life values, and U -Th isotopic measurements by multi-collector inductively coupled plasma mass spectrometry. *Earth and Planetary Science Letters* **371**, 82–91.

Colucci R, Boccali C, Žebre M and Guglielmin M (2016a) Rock glaciers, protalus ramparts and pronival ramparts in the south-eastern alps. *Geomorphology* **269**, 112–121.

Colucci R, Fontana D, Forte E, Potleca M and Guglielmin M (2016b) Response of ice caves to weather extremes in the southeastern alps, Europe. *Geomorphology* **261**, 1–11.

Colucci RR and 6 others (2017b) First alpine evidence of in situ coarse cryogenic cave carbonates (ccccoarse). *Geografia Fisica e Dinamica Quaternaria* **40**(1), 53–59.

Colucci RR and 6 others (2021) Recent increases in winter snowfall provide resilience to very small glaciers in the Julian Alps, Europe. *Atmosphere* **12**(2), 263.

Colucci RR (2016) Geomorphic influence on small glacier response to post-little ice age climate warming: Julian Alps, Europe. *Earth Surface Processes and Landforms* **41**(9), 1227–1240.

Colucci RR, Giorgi F and Torma C (2017a) Unprecedented heat wave in December 2015 and potential for winter glacier ablation in the eastern alps. *Scientific Reports* **7**(1), 7090.

Colucci RR and Guglielmin M (2015) Precipitation-temperature changes and evolution of a small glacier in the southeastern European alps during the last 90 years. *International Journal of Climatology* **35**(10), 2783–2797.

Colucci RR and Guglielmin M (2019) Climate change and rapid ice melt: Suggestions from abrupt permafrost degradation and ice melting in an alpine ice cave. *Progress in Physical Geography: Earth and Environment* **43**(4), 561–573.

Colucci RR and Žebre M (2016) Late holocene evolution of glaciers in the southeastern alps. *Journal of Maps* **12**(sup1), 289–299.

Donner A and 6 others (2023) Cryogenic cave minerals recorded 1889 CE melt event in northeast Greenland. *Climate of the Past Discussions* **2023**, 1–18.

Dublyansky YV, Moseley GE, Koltai G, Töchterle P and Spötl C (2024) Cryogenic cave carbonates. *Encyclopedia of Quaternary Science* **5**, 411–421.

Dyonisius MN and TM Jenk (2025) Ice core methods: studies of radiocarbon in ice. In S Elias (ed.), *Encyclopedia of Quaternary Science, 2nd Edn. Oxford:*. Elsevier, pp. 206–220.

Edwards RL, Chen J and Wasserburg G (1987) 238U-234U-230Th-232Th systematics and the precise measurement of time over the past 500,000 years. *Earth and Planetary Science Letters* **81**(2-3), 175–192.

Erdtman G (1960) The acetolysis method. A revised description. *Svensk Botanisk Tidskrift* **54**, 56–564.

Fang L and 9 others (2023) Early Holocene ice on the Begguya plateau (Mt. Hunter, Alaska) revealed by ice core 14C age constraints. *The Cryosphere Discussions* **2023**, 1–29.

Fang L, Jenk TM, Singer T, Hou S and Schwikowski M (2021) Radiocarbon dating of alpine ice cores with the dissolved organic carbon (doc) fraction. *The Cryosphere* **15**(3), 1537–1550.

Feng Z and 9 others (2019) Dating glacier ice of the last millennium by quantum technology. *Proceedings of the National Academy of Sciences* **116**(18), 8781–8786.

Festi D and 6 others (2015) A novel pollen-based method to detect seasonality in ice cores: a case study from the Ortles glacier, South Tyrol, Italy. *Journal of Glaciology* **61**(229), 815–824.

Festi D, Alessi N, Wellstein C, Zerbe S and Oeggl K (2023) Rapid vegetation responses over the last seven decades revealed by an alpine ice core and land-cover patterns. *Landscape Ecology* **38**(11), 2779–2793.

Festi D, Kofler W and Oeggl K (2019) Comments on Brugger and others (2018) A quantitative comparison of microfossil extraction methods from ice cores. *Journal of Glaciology* **65**(250), 344–346.

Festi D, Schwikowski M, Maggi V, Oeggl K and Jenk TM (2021) Significant mass loss in the accumulation area of the Adamello glacier indicated by the chronology of a 46 m ice core. *The Cryosphere* **15**(8), 4135–4143.

Gabrielli P and 9 others (2016) Age of the Mt. Ortles ice cores, the Tyrolean Iceman and glaciation of the highest summit of South Tyrol since the northern hemisphere climatic optimum. *The Cryosphere* **10**6, 2779–2797.

Golovko VV (2023) Application of the most frequent value method for 39Ar half-life determination. *The European Physical Journal C* **83**(10), 930.

Gu JQ and 7 others (2021) Reconstruction of the atmospheric 39Ar/Ar history. *Chemical Geology* **583**, 120480.

Hoffmann D and 9 others (2018a) U-Th dating of carbonate crusts reveals Neandertal origin of Iberian cave art. *Science* **359**(6378), 912–915.

Hoffmann DL, Pike AW, García-Diez M, Pettitt PB and Zilhão J (2016) Methods for U-series dating of CaCO3 crusts associated with palaeolithic cave art and application to Iberian sites. *Quaternary Geochronology* **36**, 104–119.

Hoffmann H and 6 others (2018b) A new sample preparation system for micro-14C dating of glacier ice with a first application to a high alpine ice core from Colle Gnifetti (Switzerland). *Radiocarbon* **60**(2), 517–533.

Holmlund P and 6 others (2005) Assessing the palaeoclimate potential of cave glaciers: the example of the Scarisoara ice cave (Romania). *Geografiska Annaler: Series A, Physical Geography* **87**(1), 193–201.

Hooghiemstra H (2004) Review of: (2004) Leitfaden der pollenbestimmung für mitteleuropa und angrenzende gebiete. *Review of Palaeobotany and Palynology* **132**.

Hou S and 7 others (2018) Age ranges of the Tibetan ice cores with emphasis on the Chongce ice cores, Western Kunlun mountains. *The Cryosphere* **12**(7), 2341–2348.

Hou S and 9 others (2025) A radiometric timescale challenges the chronology of the iconic 1992 Guliya ice core. *Science Advances* **11**(37), eadx8837.

Jenk T and 6 others (2007) Microgram level radiocarbon (14C) determination on carbonaceous particles in ice. *Nuclear Instruments and Methods in Physics Research Section B: Beam Interactions With Materials and Atoms* **259** (1), 518–525.

Jenk TM and 7 others (2006) Radiocarbon analysis in an alpine ice core: record of anthropogenic and biogenic contributions to carbonaceous aerosols in the past (1650–1940). *Atmospheric Chemistry and Physics* **6**(12), 5381–5390.

Jenk TM and 9 others (2009) A novel radiocarbon dating technique applied to an ice core from the alps indicating late Pleistocene ages. *Journal of Geophysical Research: Atmospheres* **114**(D14), D14305.

Kadebskaya OI and Mavlyudov BR (2018) Ice caves in Asia. In *Ice Caves*. Elsevier, pp. 437–454.

Karimi Vardanjani H, Bahadorinia S and Ford DC (2017) An introduction to hypogene Karst regions and caves of Iran. *Hypogene Karst Regions and Caves of the World* **1**, 479–494.

Kern Z and Perşoiu A (2013) Cave ice–the imminent loss of untapped mid-latitude cryospheric palaeoenvironmental archives. *Quaternary Science Reviews* **67**, 1–7.

Kern Z, Széles E, Horvatinčić N, Fórizs I, Bočić N and Nagy B (2011) Glaciochemical investigations of the ice deposit of Vukušić ice cave, Velebit mountain, Croatia. *The Cryosphere* **5**2, 485–494.

Kral F (1968) Pollenanalytische untersuchungen zur frage des alters der eisbildungen in der dachstein-rieseneishöhle. *Die Höhle* **19**(2).

Lauriol B and Clark ID (1993) An approach to determine the origin and age of massive ice blockages in two Arctic caves. *Permafrost and Periglacial Processes* **4**(1), 77–85.

Lauritzen SE (2006) Caves and speleogenesis at Blomstrandsøya, Kongsfjord, W. Spitsbergen. *International Journal of Speleology* **35**(1), 5.

Le Roy M and 8 others (2024) Holocene glacier variations in the alps. In *European Glacial Landscapes. The Holocene*. Amsterdam: Elsevier.

Loosli HH (1983) A dating method with 39Ar. *Earth and Planetary Science Letters* **63**(1), 51–62.

Ludwig K and Titterington D (1994) Calculation of 230Th/U isochrons, ages, and errors. *Geochimica et Cosmochimica Acta* **58**(22), 5031–5042.

Luetscher M, Borreguero M, Moseley G, Spötl C and Edwards R (2013) Alpine permafrost thawing during the medieval warm period identified from cryogenic cave carbonates. *The Cryosphere* **7**(4), 1073–1081.

Luetscher M and Jeannin PY (2004) Temperature distribution in Karst systems: the role of air and water fluxes. *Terra Nova* **16**(6), 344–350.

Maggi V, Colucci R, Scoto F, Giudice G and Randazzo L and others (2018) Ice caves in Italy-chapter 19. In Aurel P and Stein-Erik L (eds.) *Ice Caves*. Elsevier, pp. 399–423.

Malone JL, Castro MC, Hall CM, Doran PT, Kenig F and McKay CP (2010) New insights into the origin and evolution of Lake Vida, Mcmurdo Dry Valleys, Antarctica—a noble gas study in ice and brines. *Earth and Planetary Science Letters* **289**(1-2), 112–122.

Mazier F and 7 others (2009) Multidisciplinary approach to reconstructing local pastoral activities: an example from the Pyrenean mountains (Pays Basque). *The Holocene* **19**(2), 171–188.

McIntyre G, Brooks C, Compston W and Turek A (1966) The statistical assessment of Rb-Sr isochrons. *Journal of Geophysical Research* **71**(22), 5459–5468.

Mercuri AM, Mazzanti MB, Florenzano A, Montecchi MC and Rattighieri E (2013) Olea, Juglans and Castanea: the Ojc group as pollen evidence of the development of human-induced environments in the Italian peninsula. *Quaternary International* **303**, 24–42.

Mikolic U (1979) *Caverna del Ghiaccio del Monte Leupa*. Catasto Grotte - Regione Autonoma Friuli Venezia Giulia.

Moore PD, Webb JA and Collinson ME (1991) *Pollen Analysis*, 2nd Edn. Blackwell Scientific.

Munroe J, Kimble K, Spötl C, Marks GS, McGee D and Herron D (2021) Cryogenic cave carbonate and implications for thawing permafrost at Winter Wonderland Cave, Utah, USA. *Scientific Reports* **11**(1), 6430.

Nicolussi K, Le Roy M, Schlüchter C, Stoffel M and Wacker L (2022) The glacier advance at the onset of the little ice age in the alps: new evidence from Mont Miné and morteratsch glaciers. *The Holocene* **32**(7), 624–638.

Nicolussi K and Patzelt G (2000) Abhandlungen-Untersuchungen zur holozanen gletscherentwicklung von Pasterze und Gepatschferner (Ostalpen). Mit 41 abbildungen. *Zeitschrift fur Gletscherkunde und Glazialgeologie* **36**, 1–88.

Oliva M and 9 others (2018) Permafrost conditions in the mediterranean region since the last glaciation. *Earth-Science Reviews* **185**, 397–436.

Persoiu A and Lauritzen SE (2017) *Ice Caves*. Elsevier.

Perşoiu A and Pazdur A (2011) Ice genesis and its long-term mass balance and dynamics in Scărişoara ice cave, Romania. *The Cryosphere* **5**(1), 45–53.

Perşiu A, Onac BP, Wynn JG, Blaauw M, Ionita M and Hansson M (2017) Holocene winter climate variability in central and eastern Europe. *Scientific Reports* **7**(1), 1–8.

Racine TM, Reimer PJ and Spötl C (2022) Multi-centennial mass balance of perennial ice deposits in alpine caves mirrors the evolution of glaciers during the late holocene. *Scientific Reports* **12**(1), 11374.

Ramsey BC (2021) Oxcal v. 4.4. https://c14.arch.ox.ac.uk/oxcal. *OxCal. html*

Ravazzi C and 9 others (2011) Lake evolution since the Bronze Age in the Lower Mincio River valley and the Forcello Etruscan harbour (Central Po plain). *Alpine and Mediterranean Quaternary* **24**, 202–204.

Reille M (1999) *Pollen et spores d'Europe et d'Afrique du Nord*. FeniXX.

Reimer PJ and 9 others (2020) The IntCal20 Northern Hemisphere radiocarbon age calibration curve (0–55 cal kBP). *Radiocarbon* **62**(4), 725–757.

Ritterbusch F and 9 others (2022) A Tibetan ice core covering the past 1,300 years radiometrically dated with 39Ar. *Proceedings of the National Academy of Sciences* **119**(40), e2200835119.

Rowan SA, Luetscher M, Laemmel T, Harrison A, Szidat S and Lechleitner FA (2024) Subsurface co 2 dynamics in a temperate karst system reveal complex seasonal and spatial variations. *EGUsphere* **2024**, 1–48.

https://doi.org/10.1017/jog.2026.10125 Published online by Cambridge University Press

Sancho C, Belmonte A, Bartolomé M, Moreno A, Leunda M and Lopez-Martinez J (2018) Middle-to-late Holocene palaeoenvironmental reconstruction from the A294 ice-cave record (Central Pyrenees, northern Spain). *Earth and Planetary Science Letters* **484**, 135–144.

Schmeidl H and Kral F (1969) Zur pollenanalytischen altersbestimmung der eisbildungen in der schellenberger eishöhle und in der dachstein-rieseneishöhle. *Jahrbuch des Vereins zu Schutze der Alpenpflanzen und-tiere* **34**, 67–84.

Securo A, Del Gobbo C and Colucci RR (2022a) Multi-year evolution of 75 snow and ice deposits in Schachtdolines and Shafts of recently deglaciated karst terrain: Observations from Mount Canin-Kanin, Julian Alps, Europe. *Geomorphology* **417**, 108434.

Securo A, Forte E, Martinucci D, Pillon S and Colucci RR (2022b) Long-term mass-balance monitoring and evolution of ice in caves through structure from motion–multi-view stereo and ground-penetrating radar techniques. *Progress in Physical Geography: Earth and Environment* **46**(3), 422–440.

Segnana M and 9 others (2020) Holocene vegetation history and human impact in the eastern Italian alps: a multi-proxy study on the Coltrondo peat bog, Comelico Superiore, Italy. *Vegetation History and Archaeobotany* **29**, 407–426.

Shen CC and 9 others (2012) High-precision and high-resolution carbonate 230Th dating by MC-ICP-MS with SEM protocols. *Geochimica et Cosmochimica Acta* **99**, 71–86.

Sigl M and 9 others (2009) Towards radiocarbon dating of ice cores. *Journal of Glaciology* **55**(194), 985–996.

Spötl C and Cheng H (2014) Holocene climate change, permafrost and cryogenic carbonate formation: insights from a recently deglaciated, high-elevation cave in the Austrian alps. *Climate of the Past* **10**(4), 1349–1362.

Spötl C, Koltai G and Dublyansky Y (2023) Mode of formation of cryogenic cave carbonates: experimental evidence from an alpine ice cave. *Chemical Geology* **638**, 121712.

Spötl C and Koltai G (2025) Cryogenic cave carbonates: new insights from alpine ice caves. *Chemical Geology* **685**, 122808.

Töchterle P and 7 others (2022) 230Th/U isochron dating of cryogenic cave carbonates. *Geochronology* **4**(2), 617–627.

Uglietti C and 6 others (2016) Radiocarbon dating of glacier ice: overview, optimisation, validation and potential. *The Cryosphere* **10**(6), 3091–3105.

Utting N, Lauriol B, Lacelle D and Clark I (2016) Using noble gas ratios to determine the origin of ground ice. *Quaternary Research* **85**(1), 177–184.

Vermeesch P (2018) Isoplotr: a free and open toolbox for geochronology. *Geoscience Frontiers* **9**(5), 1479–1493.

Vignolo-Lutati F (1934) L'Ambrosia artemisiifolia L. in Italia. *Nuovo Giornale Botanico Italiano* **41**, 172–173.

Wedepohl KH (1995) The composition of the continental crust. *Geochimica et Cosmochimica Acta* **59**(7), 1217–1232.

Wigley T and Brown M (1976) The physics of caves. In Ford TD and Cullingford CHD (eds.), *The Science of Speleology*.

Yonge CJ, Ford D, Horne G, Lauriol B and Schroeder J (2018) Ice caves in canada. In Aurel P and Stein-Erik L (eds.), *Ice Caves*. Elsevier, pp. 285–334.

Žák K and 6 others (2012) Coarsely crystalline cryogenic cave carbonate–a new archive to estimate the last glacial minimum permafrost depth in central europe. *Climate of the Past*, **8**(6), 1821–1837.

Žák K, Onac BP and Perşoiu A (2008) Cryogenic carbonates in cave environments: a review. *Quaternary International*, **187**(1), 84–96.

Žák K, Urban J, Cılek V and Hercman H (2004) Cryogenic cave calcite from several central European caves: age, carbon and oxygen isotopes and a genetic model. *Chemical Geology*, **206**(1-2), 119–136.

Žebre M, Colucci RR, Giorgi F, Glasser NF, Racoviteanu AE and Del Gobbo C (2021) 200 years of equilibrium-line altitude variability across the European alps (1901–2100). *Climate Dynamics*, **56**(3), 1183–1201.

Žebre M and Stepišnik U (2016) Glaciokarst geomorphology of the northern dinaric alps: Snežnik (Slovenia) and Gorski Kotar (Croatia). *Journal of Maps*, **12**(5), 873–881.

https://doi.org/10.1017/jog.2026.10125 Published online by Cambridge University Press